

Design of Liquid Crystal Based Coplanar Waveguide Tunable Phase Shifter with no Floating Electrodes for 60-90 GHz Applications

J.F. Li, H. Xu and D.P. Chu*

Centre for Photonic Devices and Sensors, Department of Engineering,
University of Cambridge,
Cambridge CB3 0FA, UK
* dpc31@cam.ac.uk

Abstract — A continuously tunable millimeter wave (mm-wave) phase shifter for 60-90 GHz applications was proposed using a coplanar waveguide (CPW) structure without the use of a floating electrode (FE). In contrast to conventional CPW-FE structures, the proposed FE-free CPW device can be modulated by the nematic liquid crystal (LC) materials confined in two symmetric feeding channels. The nearly true-TEM nature of this CPW design enables wideband and low-loss operations, particularly in high frequencies up to 90 GHz. In order to optimize between high tunability and low loss, the aspect ratio of the CPW structure was optimized to maximize the defined Figure-of-Merit (FoM). By taking into account different loss mechanisms in the designed structure and the effect of LC orientations, the driving-voltage dependent impedance matching was examined to minimize the return and insertion losses. As an example, the design of a phase shifter aimed to operate at 79 GHz with low bias voltages (0-10 V) is presented, showing a wide phase shift range of 0-408° and a low insertion loss from -6.15dB to -4.56dB. The corresponding FoM is 66.3°/dB, which is expected to outperform over other LC-based phase shifters as reported within the targeted frequency range of 60-90 GHz.

Keywords—millimeter wave; tunable phase shifter; liquid crystal

I. INTRODUCTION

Steering an electromagnetic beam at 60-90 GHz is desirable for high-precision automotive radar or hand-gesture sensing. Current microwave technology using solid-state p-i-n diodes and RF MEMS [1] has a limited scope in meeting more and more stringent requirements in wavefront phase control and device performance for the cutting-edge applications in this frequency range. A main impediment to the adoption and commercialization of millimeter wave (mm-wave) phase array antenna technology at present is the lack of cost-effective phase modulating devices with high tuning efficiency, low insertion loss and continuous phasing tuning at the same time.

Working as electrically tunable dielectric materials based on shape anisotropy, nematic liquid crystals (LCs) have attracted considerable attention in recent years because of the capability of continuous phase tuning as well as low losses in comparison with ferroelectric materials at the mm-wave range [1]. Applying a small bias voltage (<10 V) can easily orient the LC molecules. The resulting variation in the effective dielectric

constant of LCs could be utilized in a guided structure to alter the propagation velocity of a microwave signal and hence continuously controlling the corresponding phase delay. The continuous phasing tuning (i.e. analog functionality) is especially useful in beam-scanning applications with improved beam-pointing accuracy.

However, limited by the current status of LC mm-wave technology in which most of the LC-based devices have been designed for <40 GHz, LC-based tunable phase shifters and other phase components are not well established in the frequency regime of 60-90 GHz. LC-based coplanar waveguide (CPW) variable phase shifters reported [2] [3] were based on tuning in the interlayer between coplanar electrodes and the floating electrode (FE) on top. This has an advantage of relatively fast electrically tuning speed due to the thin LC layer required. However, the FE-induced non-TEM nature results in high dispersion and large material absorptions as well, which precludes their applications beyond 60 GHz. Such structures even struggle to compete with a state-of-the-art inverted microstrip line [4] (assuming it of the same length). Few studies reported so far have been concerned with FE-free CPW gaps-tuning configuration with identical sheltering substrates on top and bottom (i.e. completely symmetric). Little is known about the effect of its aspect ratio on tuning range and insertion loss. There has thus far been little research into optimizing the corresponding geometry for more efficient use of LC's shape anisotropic dielectric properties.

In this work, we employ a highly anisotropic nematic LC material (GT3-24002 from Merck) as the tunable dielectric medium and design an electrically controlled phase shifter using FE-free CPW structure for the application of feeding phase array antennas operating at 79 GHz. We propose a measure to improve the tuning range and hence maximize the effective wave-occupied volume, allowing mm-wave signal to be dominantly guided in the tunable dielectric channels. The effect of CPW aspect ratio on tuning range and material absorptions was simulated in section II. In-depth analysis on diverse loss mechanisms and multi-objective optimization were presented in section III. The maximum insertion loss was reduced by designing the geometry for exact impedance match when material absorptions are at the maximum.

II. TUNING RANGE STUDY

A. Tuning Mechanism and Impact of Substrate Materials

As the schematic shown in Fig. 1, the proposed FE-free CPW with copper strip thickness (T_{strip}) of 70 μm , and channel width (W_{gap}) of 75 μm filled with the LC was modelled using LCD Master (Shintech). LC alignment was set as 90° pretwist in line with mm-wave propagating direction. Macroscopic data of the nematic LC used in this work are: $\epsilon_{r\perp}=2.5$, $\tan\delta_{\perp}=0.0123$, $\epsilon_{r\parallel}=3.3$, $\tan\delta_{\parallel}=0.0032$. By modulating the dielectric constant with applied low-frequency electric field between the core line and the grounds, wave speed going through the tunable section changes, leading to a voltage-dependent continuous phase shift as shown in Eqs. (1) and (2):

$$\Delta\Phi_{21} = (2\pi fL/c_0) * \Delta n_{eff} \quad (1)$$

$$\Delta n_{eff} = (\epsilon_{r,eff,\parallel})^{1/2} - (\epsilon_{r,eff,\perp})^{1/2} \quad (2)$$

where $\Delta\Phi_{21}$ is the differential phase shift, f is the mm-wave frequency, L is physical length of the tunable part, c_0 is light velocity in vacuum, Δn_{eff} is the maximum effective dielectric anisotropy in wave-occupied volume. Both $\epsilon_{r,eff,\parallel}$ and $\epsilon_{r,eff,\perp}$ are effective dielectric constants in wave-occupied volume of the device structure, instead of purely the permittivity of LC in two extreme states. In this regard, the tuning range (TR) of a LC-based tunable phase shifter structure is defined as Eq. (3):

$$TR = (\epsilon_{r,eff,\parallel} - \epsilon_{r,eff,\perp}) / \epsilon_{r,eff,\perp} \quad (3)$$

mm-wave travels both in LC-filled channels and sheltering substrates, thus TR is influenced by mm-wave-occupied volume in the tunable dielectric part relative to the outside non-tunable part. For a fixed LC material, TR is closely connected to device geometry (aspect ratio effect) as well as material properties of sheltering substrates interacting with mm-wave fields outside the tunable part. By ways of illustration in Figs. 2 and 3, we put Rogers RT/duroid 5880 ($\epsilon_r=2.2$) on top, whilst RO4003 ($\epsilon_r=3.55$) at bottom of a LC-filled CPW to investigate the difference of mm-wave propagating behavior in different substrate materials. Simulated TR of three designs with different substrates (but each design with identical substrate materials for top and bottom) was presented in Fig.4.

When the frequency increases towards 90 GHz, there is clearly a large proportion of mm-wave-occupied volume in the non-tunable 4003 substrate, whereas this phenomenon is less pronounced for 5880 with smaller dielectric constant. Note that LC permittivity decreases gradually with frequency. This exacerbates the mm-wave dispersed into substrates with high permittivity, and hence degrading TR as evidenced by Fig. 4. Thus 5880 substrates were used in this work (see Fig. 1).

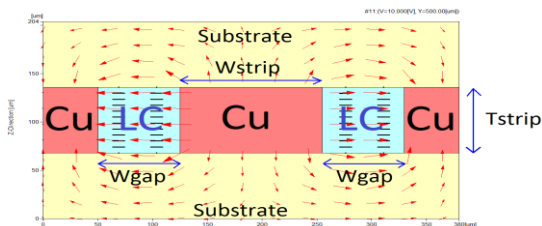


Fig.1. Sketch of the proposed LC-based CPW (cross-sectional view).

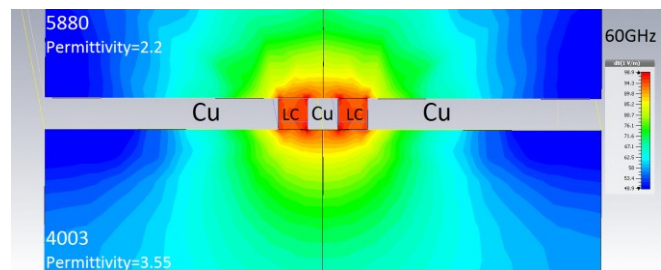


Fig.2. mm-wave field strength distribution at 60 GHz (input power = 1W).

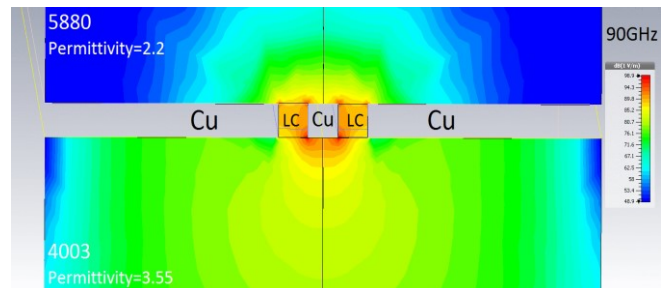


Fig.3. mm-wave field strength distribution at 90 GHz (input power = 1W).

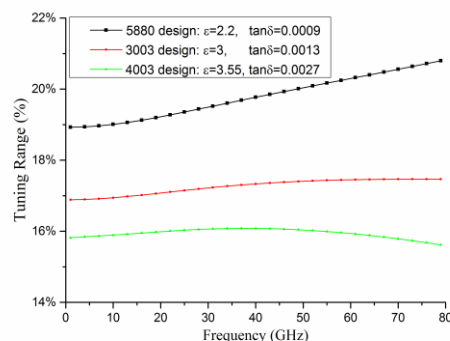


Fig.4. Dispersion of TR for CPW designs using different substrates.

B. Aspect Ratio Effect on Modes and TR

Geometry-dependent CPW mode affects the mm-wave-occupied volume ($W_{oV_{eff}}$) within the tunable channels and hence the TR. As depicted in Fig. 5, we performed simulations and obtained a library of TR parametrized with respect to T_{strip} and W_{gap} . Aspect ratio (AR), defined as the ratio of T_{strip} and W_{gap} in Fig. 6, was used to further investigate the geometry size effect (compared to wavelength) on modes evolution and TR.

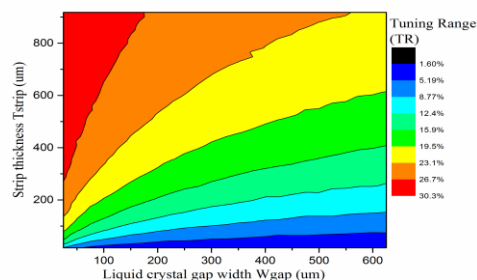


Fig.5. Effect of geometry size on TR (79 GHz, 10 V bias).

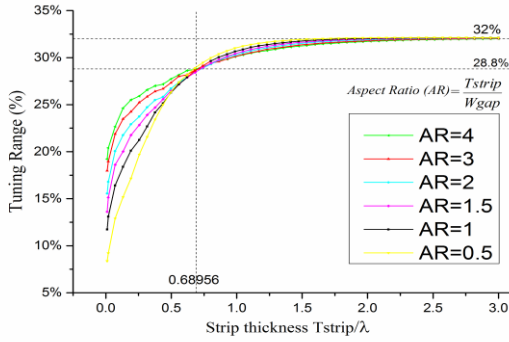


Fig. 6. TR vs. T_{strip} at different AR (79 GHz, 10 V bias).

As shown in Fig. 6, the rise of T_{strip} increases $W_{oV_{eff}}$ and hence improves TR due to mitigation of radiation outside the tunable channels. When $T_{strip} \ll \lambda/2$, higher AR (i.e. narrower W_{gap}) leads to larger TR before TR begins to saturate when $T_{strip} \approx \lambda/2$, as the generation of TE_{10} mode and 2D propagation partially reduces $W_{oV_{eff}}$. Specifically, we observed that W_{gap} loses impact at $T_{strip} \approx 2\lambda/3$, where each AR design exhibits the same TR (28.8%). When $T_{strip} > 2\lambda/3$, the trend even reverses (i.e. lower AR, larger TR), but finally all level off at 32%, with minor difference observed. To quantify the modes transition effect, we presented TR vs. AR (varying W_{gap} for each T_{strip}) in Fig. 7 (a). With $T_{strip} \ll \lambda/2$, the proposed CPW exhibits a nearly true-TEM mode, TR rises almost linearly with AR, as the tuning capacitance per unit length is governed by Eq. (4):

$$C = \epsilon_{r,eff} * T_{strip} / W_{gap} = \epsilon_{r,eff} * AR \quad (4)$$

With T_{strip} rising towards $\lambda/2$, mm-wave field pattern variations become pronounced along the strip height, as TE_{10} mode begins to dominate each channel. The rate of change in TR with AR drops gradually to 0, and turns negative with $T_{strip} > 2\lambda/3$.

III. LOSS ANALYSIS AND OPTIMIZATION

Material absorption losses include the loss in the volume of LC and loss at the surface of copper. For $T_{strip} \ll \lambda/2$, each LC channel can be modelled as a parallel plate capacitor with lossy dielectrics as shown by Eq. (5):

$$LC \text{ Loss} = 2\pi f \epsilon_r'' V^2 L * AR = 2\pi f \epsilon_r'' (V/W_{gap})^2 T_{strip} W_{gap} L \quad (5)$$

where ϵ_r'' denotes the imaginary part of LC permittivity, which is driving-voltage dependent. V/W_{gap} is mm-wave field strength (not the driving voltage field), and $T_{strip} W_{gap} L$ represents the volume of each LC-filled channel. Increasing AR for TR improvement is arguably limited by increased dielectric losses.

Figure-of-Merit (FoM), i.e. ratio of largest phase shift and largest insertion loss, was presented in Fig. 7 (b). To preclude impedance mismatching loss into this analysis, our calculations at this stage were based on treating the wave-ports excitation as without renormalization to the impedance of connectors. Based on this assumption, FoM increases with T_{strip} before the start of saturation at $T_{strip} \approx 2\lambda/3$. The maximum theoretically possible FoM (520°/dB) for 79 GHz is reached at $T_{strip} \approx 2\lambda$.

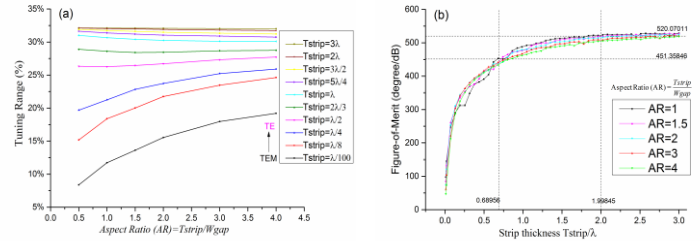


Fig. 7. (a) TR vs. AR (79 GHz, 10 V bias), and (b) FoM vs. T_{strip} (79 GHz).

Within the constraints of commercially available substrates and limited by the tolerances of manufacturing processes, we employed RT/duroid 5880 substrates with largest metallization thickness of 70 μm in this work. In this case, we obtained the optimum $W_{gap} = 75 \mu\text{m}$ for highest FoM at 79 GHz, as depicted in Fig. 8 (a). As presented in Fig. 8 (b), the optimum operating characteristic impedance Z was derived as 50 Ω for highest FoM at 79 GHz.

A. Driving-voltage Dependent Impedance Matching

As already noted in Eq. (5) above, for a fixed geometry, volume loss in LC depends on driving voltage, i.e. largest at 0V (tangential state) and smallest at 10 V (homeotropic state). During 0-10 V tuning for 0- 2π phase modulation, the voltage-dependent dielectric constant of LC gives rise to impedance variations, and hence the cause of voltage dependent return loss. In this regard, we studied into total loss minimization by exactly matching the design at a suitable bias voltage so that the largest insertion loss is reduced. We implemented this concept by slightly varying the copper strip width (W_{strip}) for impedance fine tuning, whilst keeping $T_{strip} = 70 \mu\text{m}$ and $W_{gap} = 75 \mu\text{m}$ as optimum AR. Note that the tuning of W_{strip} would also change metal loss due to the variation of copper surface area. Simulated driving-voltage dependent material absorption, reflection and transmission of a design matched at 0 V bias were presented in Fig. 9.

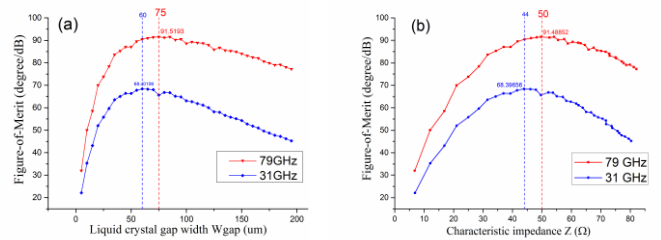


Fig. 8. (a) FoM vs. W_{gap} , and (b) FoM vs. Z (both for $T_{strip} = 70 \mu\text{m}$).

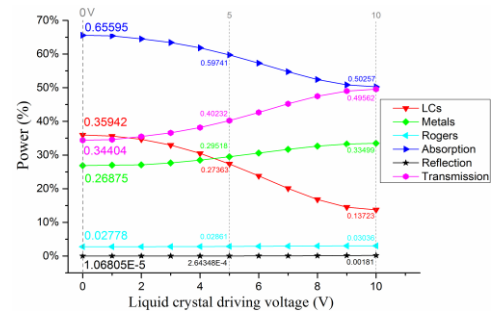


Fig. 9. Loss decomposition analysis for the 0V bias matched design.

For this FE-free CPW structure, reflection loss is too small to tip the balance, despite matching at which bias voltage. Total absorption loss predominately follows the trend of LC loss, and largest insertion loss (lowest transmission) always occurs at 0 V bias. Therefore, we strategically matched our design at 0 V (i.e. $W_{strip}=134 \mu\text{m}$), so that the largest insertion loss was minimized compared to matching at other bias voltages.

B. Connector Compensation and Whole Device Performance

The phase shifter section at each end (without LC) was designed as a quarter-wave transformer for matching and also for accommodating transition blocks of CPW connectors. For impedance mismatching due to height discontinuity between connector launch pin and the CPW strip underneath, we employed two approaches to compensate for the parasitic capacitance at the transition section (as sketched in Fig. 10), with the results outlined in Table I. Compared with tapering, the right-angle compensation better addresses mismatching and exhibits lowest insertion loss, although with slightly higher radiation.

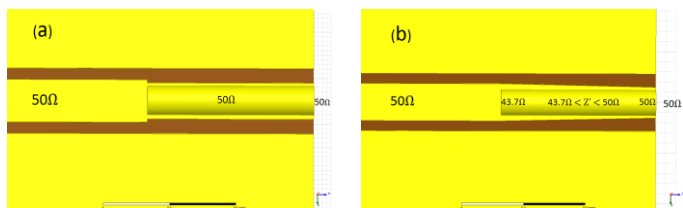


Fig.10. Two compensation scenarios: (a) right-angle, and (b) tapering.

TABLE I. ADDRESSING MISMATCHING WITH CONNECTOR PINS

| Solutions | At 79 GHz with 0 V bias | | |
|--------------------------|-------------------------|----------|-----------|
| | S21 | S11 | Radiation |
| No compensation | -5.4 dB | -16.9 dB | -17.4 dB |
| Right-angle compensation | -5.3 dB | -31.3 dB | -15.2 dB |
| Tapering compensation | -5.3 dB | -26.8 dB | -15.3 dB |

The complete device structure (LC channel length=4.5cm) and its performance with connectors were presented in Figs. 11 and 12. As summarized in Table II, our design presents a tangible improvement in the overall performance when compared with that of a recent work [5].

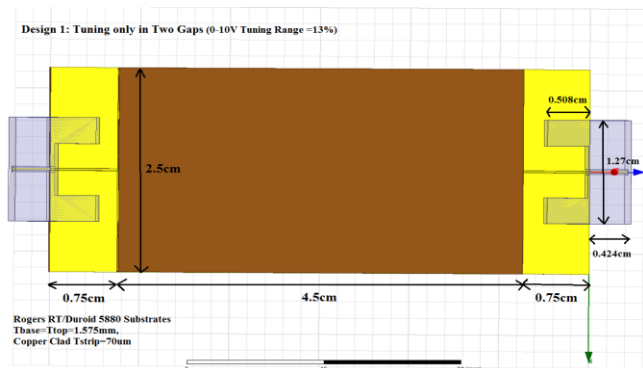


Fig.11. Final design of the LC-based CPW phase shifter without FE.

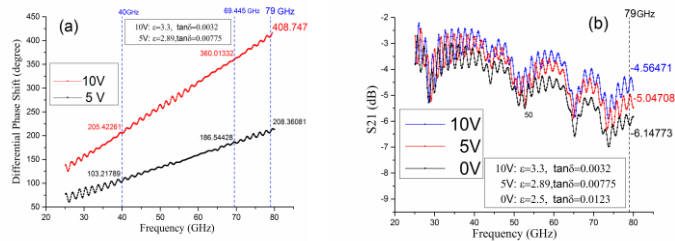


Fig.12. Performance of the proposed design (LC channel length=4.5cm): (a) differential phase shift, and (b) insertion loss including connectors.

TABLE II. PROPOSED DESIGN VS. STATE-OF-THE-ART AT 79 GHz

| LC-based CPW Phase Shifters | Phase Shift | Insertion Loss | FoM |
|-----------------------------|---------------------------|----------------|---------|
| [5] | 100° | -2.40 dB | 42 °/dB |
| This work | LC channel length = 1.1cm | -1.99 dB | 50 °/dB |
| | LC channel length = 4.5cm | -6.15 dB | 66 °/dB |

IV. CONCLUSION

A novel LC-based mm-wave CPW phase shifter in the 60-90 GHz range with no floating electrodes was proposed. It showed a 20% increase in the FoM over other reported devices. Design optimization includes the tuning range improvement by considering the effect of aspect ratios on the mm-wave field distribution, the insertion loss minimization by systematically analyzing the effects of various loss mechanisms as well as introducing the driving-voltage dependent impedance matching strategy. These make the proposed phase shifter potentially capable of to fulfil the application requirements of broadband phase antenna arrays in this frequency range.

REFERENCES

- [1] A.Franc, O.Karabey, G.Rehder, E.Pistono, R.Jakoby and P.Ferrari, "Compact and broadband millimeter-wave electrically tunable phase shifter combining slow-wave effect with liquid crystal technology," IEEE Transactions on Microwave Theory and Techniques, ISSN 0018-9480, 2013, Volume 61, Issue 11, pp. 3905 – 3915
- [2] T.Nguyen, S.Umeno, H.Higuchi, H.Kikuchi, H.Moritake, "Improvement of decay time in nematic-liquid-crystal-loaded coplanar-waveguide-type microwave phase shifter by polymer stabilizing method," Japanese Journal of Applied Physics, ISSN 0021-4922, 01/2014, Volume 53, Issue 1, pp. 01AE08 - 1-01AE08-6
- [3] Y.Utsumi, T.Kamei, T.Maeda and N.Dinh, "Microwave high-speed liquid crystal devices using CPW with floating electrode," Molecular Crystals and Liquid Crystals, ISSN 1542-1406, 12/2007, Volume 476, Issue 1, pp. 3/[249] - 13
- [4] Y. Garbovskiy, V. Zagorodnii, P. Krivosik, J. Lovejoy, R. E. Camley, Z. Celinski, A. Glushchenko, J. Dziaduszek and R. Dąbrowski, "Liquid crystal phase shifters at millimeter wave frequencies," J. Appl. Phys. ISSN 0021-8979, 03/2012, Volume 111, Issue 5, pp. 054504 - 054504-4
- [5] C.Fritsch, F.Giacomozzi, O.Karabey, S.Bildik, S.Colpo and R.Jakoby, "Advanced characterization of a W-band phase shifter based on liquid crystals and MEMS technology", International Journal of Microwave and Wireless Technologies, ISSN 1759-0787, 06/2012, Volume 4, Issue 3, pp. 379 - 386